ACS OMEGA

Open Access

http://pubs.acs.org/journal/acsodf

Article

Tunable Periodic Nanopillar Array for $MAPbI_3$ Perovskite Photodetectors with Improved Light Absorption

Zhengtong Yao, Yuting Xiong, Hanyue Kang, Xiuzhen Xu,* Jianhe Guo,* Wen Li,* and Xiaobin Xu*

Cite This: *ACS Omega* 2024, 9, 2606−2614

Read Online

ACCESS | Metrics & More | Article Recommendations | Supporting Information

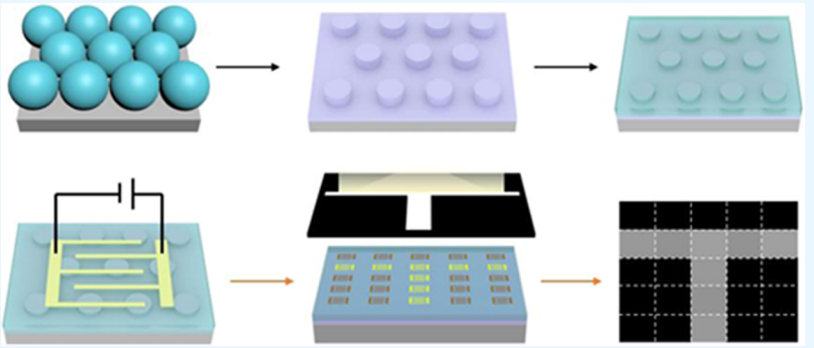

ABSTRACT: In the field of optoelectronic applications, the vigorous development of organic−inorganic hybrid perovskite materials, such as methylammonium lead triiodide ($MAPbI_3$), has spurred continuous research on methods to enhance the photodetection performance. Periodic nanoarrays can effectively improve the light absorption of perovskite thin films. However, there are still challenges in fabricating tunable periodic patterned and large-area perovskite nanoarrays. In this study, we present a cost-effective and facile approach utilizing nanosphere lithography and dry etching techniques to create a large-area Si nanopillar array, which is employed for patterning $MAPbI_3$ thin films. The scanning electron microscopy (SEM) and X-ray diffraction (XRD) results reveal that the introduction of nanopillar structures did not have a significant adverse effect on the crystallinity of the $MAPbI_3$ thin film. Light absorption tests and optical simulations indicate that the nanopillar array enhances the light intensity within the perovskite films, leading to photodetectors with a responsivity of 11.2 A/W and a detectivity of 7.3×10^{10} Jones at 450 nm in wavelength. Compared with photodetectors without nanostructures, these photodetectors exhibit better visible light absorption. Finally, we demonstrate the application of these photodetector arrays in a prototype image sensor.

1. INTRODUCTION

Photodetectors that convert incident light (ultraviolet, visible, or infrared) into electrical signals are pivotal in numerous industrial and scientific fields, including optical communication, environmental monitoring, day and night monitoring, and chemical and biological sensing.[1−3] For high-performance photodetection, materials with low cost, high optical absorption coefficient, narrow direct band gap, and fast response rate are imperative.[4−6] Many materials have been explored for photon detection, including graphene,[7−9] colloidal nanocrystals,[10−12] metal oxides,[13−15] and metal halide perovskites and their hybrids.[16−18] In particular, organic−inorganic hybrid perovskites, such as methylammonium lead trihalide ($MAPbX_3$, where MA = CH_3NH_3, X = Cl, Br, or I), have gained increasing attention due to their high optical absorption coefficient, carrier mobility, and long diffusion length over a wide spectral range.[19−21] Thus, they are considered a promising candidate for next-generation photodetection applications. In recent years, people have been continuously striving to optimize surface defects, control crystal growth, and improve light-trapping ability of organic−inorganic hybrid perovskite films to optimize the performance of photodetectors.[22−24]

Although metal halide perovskite exhibits excellent performance for high-performance photodetectors, their susceptibility to moisture and oxygen in the air can curtail their potential applications,[25] and the grain boundary effect and internal decomposition have a significant impact on the performance of perovskite devices. These defects are prone to appear at the interface and grain boundaries of perovskite films, which reduce the probability of radiation recombination and lead to trap states related to grain boundaries.[26,27] Therefore, it is critical to slow down the decomposition process and improve

Received: September 25, 2023
Revised: November 29, 2023
Accepted: November 30, 2023
Published: January 2, 2024

https://doi.org/10.1021/acsomega.3c07390
ACS Omega 2024, 9, 2606−2614

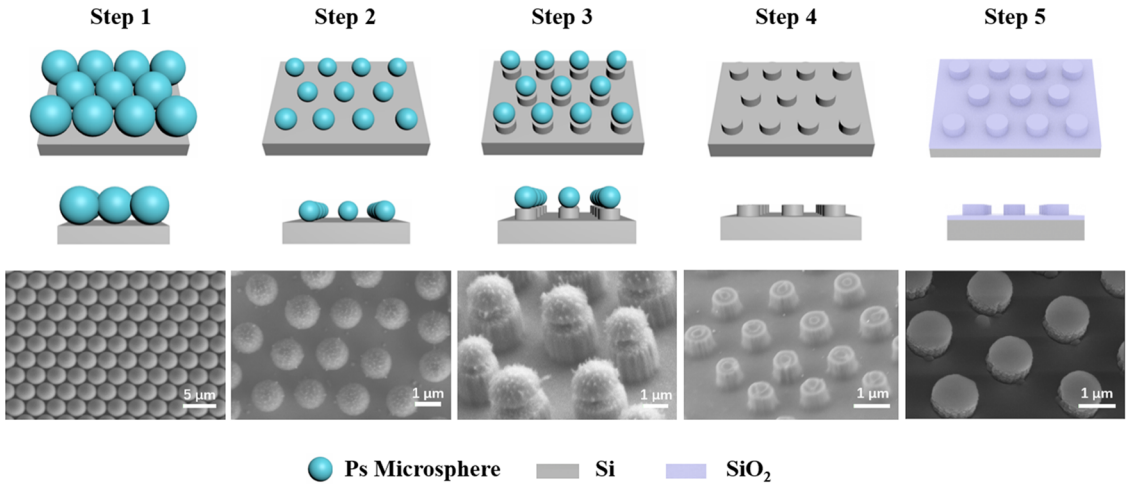

Figure 1. Schematic diagram of the produced nanopillar array by microsphere lithography, dry etching, and related scanning electron microscopy images. Step 1: spread a single layer of polyethylene (PS) spheres onto a Si substrate (top view SEM). Step 2: reduced the diameter of the PS spheres via O_2 plasma etching (top view SEM). Step 3: fabricated nanopillars' structures via dry etching (45° top view SEM). Step 4: removed the PS spheres on the nanopillars via oxygen plasma (45° top view SEM). Step 5: evaporated a 200 nm-thick SiO_2 layer onto Si nanopillars (45° top view SEM).

the stability and performance of the device.[28,29] For instance, Jeong et al. used pseudo-halide anionic formate ($HCOO^-$) to suppress anionic vacancy defects present at grain boundaries and perovskite film surfaces, improving the film's crystallinity.[30] Wu et al.[31] incorporated 1-butyl-3-methylimidazolium tetrafluoroborate (BMIMBF4) as an additive into methylammonium lead triiodide ($MAPbI_3$) nanowires, effectively passivating defects, inhibiting the degradation of perovskite, and leading to the formation of nanochannels, achieving rapid charge transfer. Other methods such as introducing a polymer modification[32] and using a two-step imprinting technique[33] have been shown to enhance the stability of films.

The light absorption ability of the films greatly affects the performance of photodetectors. By properly designing periodic light capture nanostructures, light scattering can be increased, resulting in enhanced light absorption ability, which can improve the performance of the photodetectors.[34,35] Although periodic nanoarray structures exhibit good repeatability and tunability compared with nonordered nanostructures, manufacturing large-area periodic arrays such as nanowires and nanotubes generally requires complex and expensive commercial lithography techniques such as electron beam lithography or focused ion beam lithography. Therefore, to achieve high-performance nanostructured organic−inorganic hybrid perovskite photodetectors on an affordable scale, it is necessary to explore and develop economical nanomanufacturing methods.

In recent years, various methods such as orthogonal lithography,[36,37] nanosphere lithography,[38−40] chemical stripping lithography,[41] self-collapse lithography,[42] nanoimprint methods,[43−45] and photolithography[46] have been developed to prepare large-area submicrometer patterns. These strategies have low cost and high repeatability and have been widely used to fabricate nanostructured devices.[47−49] For instance, Wang et al. realized a high-performance patterned perovskite photodetector at the nanometer level through nanoimprint lithography; the crystallinity and optical properties of the perovskite have been improved, which contribute to higher mobility, longer diffusion length, and better photon absorption.[50] By rationally designing light-trapping nanostructures, the crystallinity and light absorption of perovskite films can be increased, leading to improved device performance.[51]

In this work, utilizing nanosphere lithography and dry etching, we prepared a large-area-ordered nanopillar array structure for fabricating organic−inorganic hybrid perovskite films. The diameters, heights, and pitch of the nanopillars can be precisely controlled. Through spin coating, we deposited the $MAPbI_3$ thin film to fill and cover the entire periodic nanopillar array, thus enhancing the light absorption and photoelectric sensitivity of the photodetectors. Additionally, we further studied the effect of the periodic nanopillar array through a COMSOL multiphysics simulation. To demonstrate our method, we fabricated an image sensor composed of a 5 × 5 photodetector array that exhibited good imaging functionality. This strategy not only improves the photoelectric performance of the device with good repeatability but also provides a basis for the development of large-area nanostructured organic−inorganic hybrid perovskite thin-film photodetectors.

2. MATERIALS AND METHODS

2.1. Materials. Polystyrene (PS) spheres with sizes from 500 nm to 2 μm were purchased from Rigor Bioscience Development Inc. Methylammonium lead iodide ($CH_3NH_3PbI_3$) was purchased from Xi'an Polymer Light Technology Corp. All of the materials and reagents were used as received.

2.2. Fabrication of Nanopillar Arrays. Si substrates were cleaned with isopropyl alcohol, acetone, and deionized water for 10 min and dried using a nitrogen gas gun. Then, the cleaned Si substrates were treated using an oxygen plasma cleaner at 150 W for 600 s. Then, the substrates were covered with a tightly packed monolayer of PS spheres. The diameters of the PS spheres were reduced by oxygen plasma at 200 W. Dry etching was performed in a gas atmosphere of C_4F_8 and SF_6 for 2 min to obtain nanopillars. The PS spheres were eliminated on the nanopillar through 5 min of oxygen plasma. Finally, silicon dioxide with a thickness of 200 nm was deposited on the surface of the Si substrate with the nanopillar array by thermal evaporation.

https://doi.org/10.1021/acsomega.3c07390
ACS Omega 2024, 9, 2606−2614

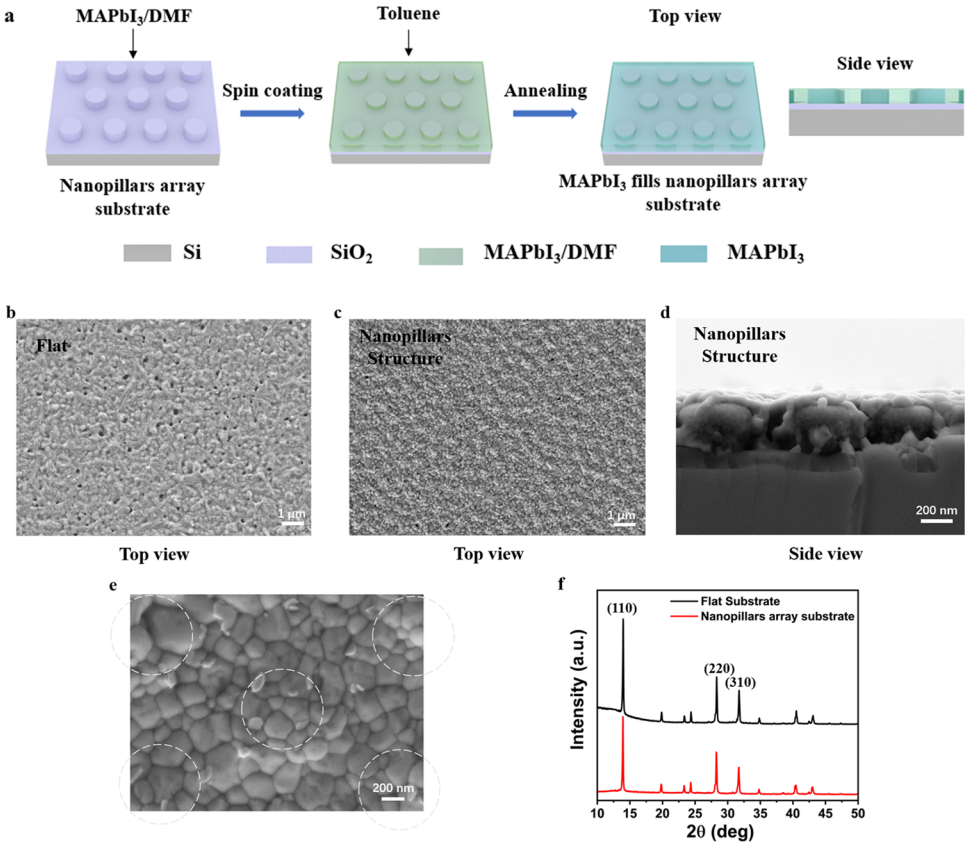

Figure 2. (a) Schematic coating process of the $MAPbI_3$ film on nanopillar arrays of SiO_2/Si. (b) Typical SEM images of the $MAPbI_3$ film fabricated on the flat substrate (top view). (c, e) Typical SEM images of the $MAPbI_3$ film fabricated on the nanopillar substrate (top view). (d) Cross-sectional SEM image of the $MAPbI_3$ film on the nanopillar substrate (side view). (f) XRD patterns of the $MAPbI_3$ film based on the nanopillar array substrate and flat substrate.

2.3. Fabrication of $MAPbI_3$ Thin Film on Nanopillar Substrates. 50 μL portion of 1 M $MAPbI_3$ perovskite precursor solution in *N*,*N*-dimethylformamide was spin-coated on the nanopillar substrate at 3000 rpm for 45 s. During spin coating, 100 μL of toluene was added dropwise on the substrate. Then, the sample was annealed at 100 °C for 10 min to form $MAPbI_3$ on the nanopillar substrate.

2.4. Fabrication of Perovskite Photodetectors. The electrodes of the photodetectors were fabricated by thermal evaporation of copper under a shadow mask, which had a thickness of 200 nm. Photodetectors based on S-1, S-2, S-3, and flat samples were fabricated under identical conditions.

3. RESULTS AND DISCUSSION

3.1. Preparation of SiO_2/Si Nanopillar Substrates. We combine nanosphere lithography and dry etching techniques to fabricate a large-area periodically tunable nanopillar array on silicon wafers and then evaporate a SiO_2 layer onto Si nanopillars, which serves as a substrate for $MAPbI_3$ thin films, as illustrated in Figure 1.

3.1.1. Step 1. Spread a single layer of polyethylene (PS) spheres with diameters of 2 μm, 1 μm, and 500 nm onto a Si (100) substrate to form a dense stack and submicrometer features.

3.1.2. Step 2. The diameters of the PS spheres were reduced by half via oxygen plasma for 30 (for 500 nm diameter PS nanospheres), 75 (for 1 μm diameter PS microspheres), and 180 s (for 2 μm diameter PS microspheres) (Figure 1 as well as Figures S1 and S2 in the Supporting Information).

3.1.3. Step 3. Low aspect ratio Si nanostructures with smooth sidewalls were directly obtained via dry etching, which simultaneously used C_4F_8 and SF_6 as etching and passivation gases for 2 min.

3.1.4. Step 4. The PS spheres on the nanopillars were removed via oxygen plasma for 5 min, exposing a large area of periodic nanopillars with diameters of 1 μm, 500 nm, and 250 nm and a height of 400 ± 30 nm (Figures S3 in the Supporting Information).

3.1.5. Step 5. A 200 nm-thick SiO_2 layer was evaporated onto the Si nanopillars by thermal vapor deposition. Then, a large area of the SiO_2/Si nanopillar array with diameters of 1 μm, 500 nm, and 250 nm was fabricated (Figure S4 in the Supporting Information).

3.2. Preparation of $MAPbI_3$ Thin Films. When the preparation of the nanostructured substrates was complete, $MAPbI_3$ was spin-coated on the SiO_2/Si substrate with nanopillars and the flat SiO_2/Si substrate, respectively. During spin coating, toluene was added dropwise as an antisolvent to promote the crystallization of $MAPbI_3$, followed by a thermal annealing process to increase crystallinity (Figure 2a). (More details are in the Supporting Information.)

As shown in Figure 2b, the $MAPbI_3$ thin film on the flat substrate does not have a specific submicrometer structure, and there are some pores on the surface (Figure S5). On the contrary, due to the periodic distribution of the nanopillar array, Figure 2c shows that the thin film with nanopillars exhibited a large-area patterned periodic morphology (Figure S5). The $MAPbI_3$ thin film completely covered the entire

https://doi.org/10.1021/acsomega.3c07390
ACS Omega 2024, 9, 2606−2614

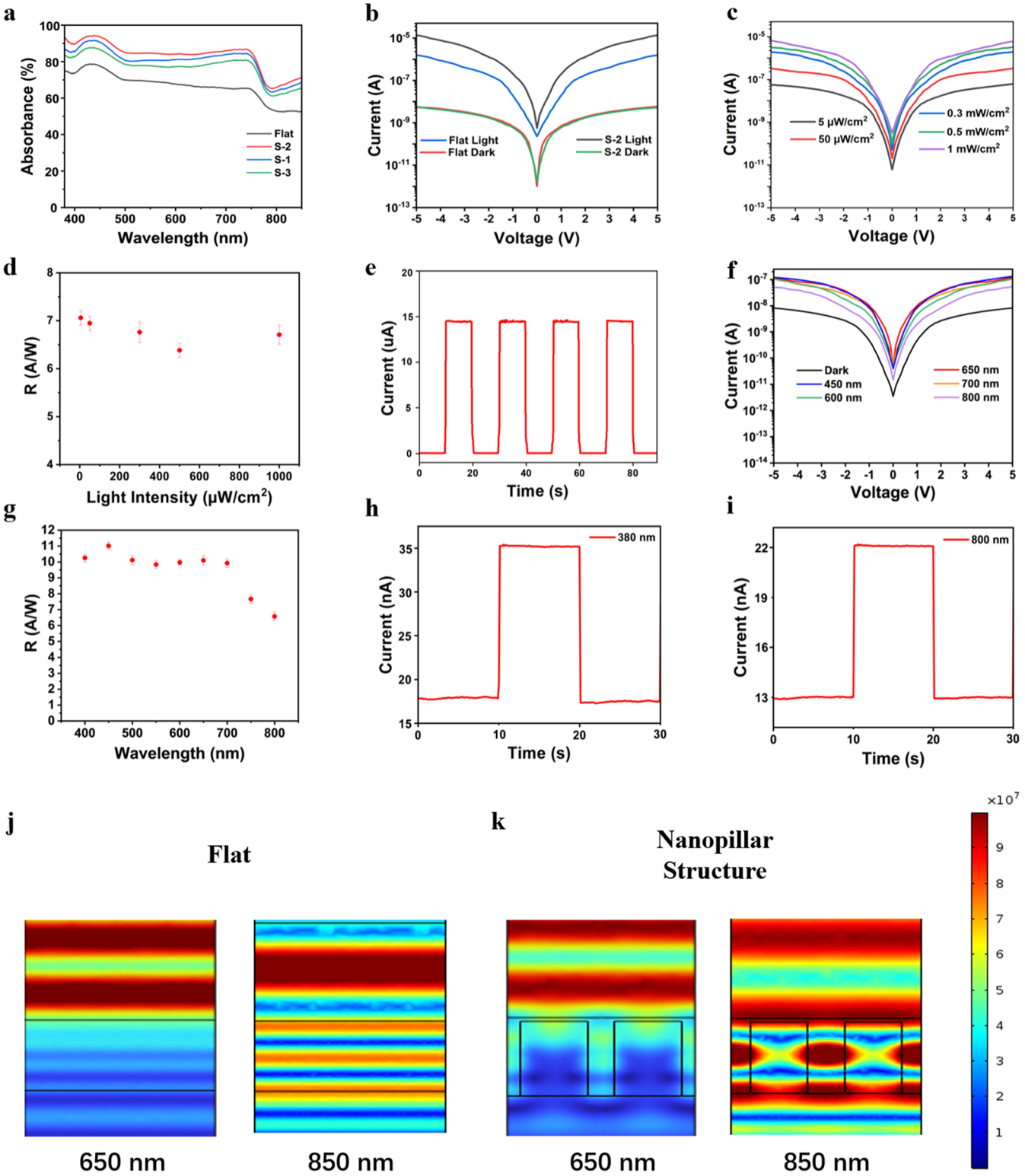

Figure 3. (a) Measured absorption spectra of $MAPbI_3$ films on SiO_2/Si nanopillar substrates and flat substrates from 380 to 850 nm. (b) Dark/photocurrent of the photodetectors based on flat substrates and nanopillar substrates. The incident white light intensity is 2.5 mW/cm^2. (c) $I-V$ curves of the photodetector (sample S-2) measured in the dark and under white light illumination with a range of light intensity. (d) Plots of responsivity of the photodetector (sample S-2) as a function of light intensity under white light. (e) Time-resolved photoresponse of the photodetector; the incident light intensity is 2.5 mW/cm^2. (f) $I-V$ curves of the S-2 at different wavelengths; the incident light intensity is 10 μW/cm^2. (g) Plots of responsivity of the photodetector (sample S-2) as a function of light intensity at different wavelengths; the incident light intensity is 10 μW/cm^2. (h, i) Time-resolved photoresponse of the photodetector at 380 and 800 nm, respectively. The incident light intensity is 10 μW/cm^2. (j, k) Magnitude of the electric field obtained from COMSOL simulations for $MAPbI_3$ films on flat substrates and SiO_2/Si nanopillar substrates under light illumination at 650 and 850 nm.

https://doi.org/10.1021/acsomega.3c07390
ACS Omega 2024, 9, 2606−2614

nanopillar array, with a thickness of 450 nm (Figure 2d), which is relatively dense, with uniform grain distribution (Figure 2e); a histogram of the particle size distribution is shown in Figure S6. Through SEM images and particle size distribution histograms, we can find that the particle sizes of the $MAPbI_3$ thin film based on different substrates are relatively similar without significant differences. X-ray diffraction patterns (XRD) of the $MAPbI_3$ thin films on different substrates are shown in Figure 2f. The diffraction pattern shows peaks among the following angles: 14.1, 28.5, 31.9, 40.5, and 43.2°, which correspond to the (110), (220), (310), (224), and (314) planes, as reported previously.[52−54] From the results of XRD (details in Supporting Information), we confirm that the crystallinity of the $MAPbI_3$ thin film does not significantly change due to the introduction of nanostructures. From the energy-dispersive spectrometer (EDS), we can see that the $MAPbI_3$ film on the nanopillar substrate shows good element distribution (Element: I, O, Pb, Si, C, and N) (Figure S7).

3.3. Performance of Photodetector Devices. In all subsequent tests and characterizations, we selected three sizes of nanopillar samples, each with at least 5 samples. Tested the following dimensions: S-1 sample, a nanopillar array with a diameter of 1000 nm; S-2 sample, a nanopillar array with a diameter of 500 nm; S-3 sample, a nanopillar array with a diameter of 250 nm; a flat SiO_2/Si substrate. Then, we prepared $MAPbI_3$ thin films on these substrates (Figure S8 in the Supporting Information) and evaporated copper electrodes to prepare devices for subsequent testing. First, we tested the absorption spectra of $MAPbI_3$ grown on different substrates (S-1, S-2, S-3, flat substrate) to examine its light absorption ability. From the results, we found that compared to the flat substrate, the absorbance of $MAPbI_3$ thin films on the substrates with nanopillar structure increased by ∼10% (Figure 3a). These results have been reported in previous reports,[16,51,55−57] indicating that in the visible light range, the introduction of nanopillars' structure can increase the scattering and decrease the reflection of light within the $MAPbI_3$ film, thus enhancing the light absorption of $MAPbI_3$ film. From the PL spectrum (Figure S9), the absorption edge around 750 nm is related to the optical absorption of the perovskite as well as the PL peak at around 780 nm. These results are consistent with those found in the scientific literature.[58]

Then, we designed and fabricated a photodetector array to test the photoelectronic characteristics of devices based on nanopillar array substrates. To prevent mutual influence between different devices, the interdigital electrode of our designed photodetector has an aspect ratio of 1/41. (The channel length and width of the photodetector are 50 and 2050 μm, respectively, Figure S10.) Figure 3b shows photodetectors' typical current versus voltage (I−V) curves based on S-2 and flat substrate measured in the dark and under white light illumination at 2.5 mW/cm^2. The photodetectors based on S-2 samples showed considerably higher current (I_{light} = 1.42 × 10^{-5} A) under white light illumination, which is 2317 times larger (at 5 V bias) than that in the darkness (I_{dark} = 6.12 × 10^{-9} A), while the photodetectors with flat substrate just showed 253 times larger (at 5 V bias) current under the same illumination (I_{light} = 1.53 × 10^{-6} A) as that in the darkness (I_{dark} = 6.04 × 10^{-9} A), which is similar to prior reports.[59−61] We also measured S-1 and S-3 samples and observed similar photocurrents to S-2 samples (Figure S11). Therefore, we found that the introduction of nanopillar array substrates can improve the photoelectric performance of $MAPbI_3$ thin film devices. These photodetectors have good stability, which exhibited stable performance after 72 h of exposure to air (Figure S12).

We further investigated the incident light intensity dependence of photodetectors. Figure 3c depicts the I−V curves measured by a photodetector based on S-2 under visible light and dark conditions with different light intensities. The light intensity of white light is 5, 50, 0.3, 0.5, and 1 mW/cm^2, respectively.

In photodetectors, the responsivity (R) represents the signal strength under illumination, which can be calculated using

$$R = \frac{J_{ph} - J_{dark}}{L_{light}} \quad (1)$$

Here, J_{ph} is the photocurrent density, J_{dark} is the dark current density, and L_{light} is the incident light intensity.[62]

From eq 1, the R values of the photodetectors based on nanopillar substrates (S-2 samples) are calculated to be 7.1 A/W (under white light at 5 μW/cm^2) (Figure 3d). Figure 3e shows the On−Off diagram measured by a photodetector based on the S-2 sample under white light at 2.5 mW/cm^2; the I_{light} and I_{dark} remain stable every 10 s, which represents the device demonstrating good optoelectronic performance stability. And we tested the I−V curves of the photodetector based on the S-2 sample measured under visible light at different wavelength under 10 μW/cm^2 and darkness (Figure 3f), and the R values at different wavelengths are shown in Figure 3g.

The specific detectivity (D^*) is often used to represent the ability of a photodetector to detect weak signals, which can be calculated through the following expression

$$D^* = \frac{(A \cdot f)^{0.5}}{(I_n/R)} \approx \frac{R}{(2q \cdot J_{dark})^{0.5}} \quad (2)$$

Here, A is the effective area of the device, f is the electrical bandwidth, I_n is the noise current, and q is the fundamental unit of charge. The D^* value of the photodetector based on S-2 is 7.3 × 10^{10} Jones (at 450 nm). The D^* values of the photodetector are distributed from 4.1 × 10^{10} to 4.6 × 10^{10} Jones under a white light intensity range from 5 to 1 mW/cm^2, which suggests that the device is sensitive to weak light.

The photodetectors based on nanopillar array substrates showed a high sensitivity to visible light, as shown in Figure 3h (under 10 μW/cm^2 at 380 nm) and Figure 3i (under 10 μW/cm^2 at 800 nm), which indicates that nanostructures can increase the light absorption in the visible light range.

As Table 1 shows, both R and D^* values of the photodetectors based on nanopillar array structures are at a good level in the photodetectors based on $MAPbI_3$ films.

To further study the photoresponse enhancement effect of the nanopillar array on $MAPbI_3$ thin film devices, we made use of optical simulations via COMSOL methods to investigate their optical properties. We simulated the electric field distribution of $MAPbI_3$ thin films on SiO_2/Si nanopillar substrates and flat substrates, respectively. (The incident light was set at 650 nm and 850 nm on the nanopillars with a height of 400 ± 30 nm and a diameter of 300 nm.) Figure 3k shows the enhancement of the electric field between nanopillar structures and periodic fluctuations along the nanopillar array, as the nanopillar array allows for repeated reflections of

https://doi.org/10.1021/acsomega.3c07390
ACS Omega 2024, 9, 2606−2614

Table 1. Comparison of the Key Parameters of Photodetectors Based on Different Materials

Material	Light source	R (A/W)	D^* (Jones)	Refs
$MAPbI_3$ nanopillars	White light	7.1	2.9×10^{10}	this work
$MAPbI_3$ nanopillars	450 nm	11.2	7.3×10^{10}	this work
$MAPbI_3$ film	White light	0.2		ref 63
	670 nm	0.3		ref 64
	365 nm	3.5		ref 65
$MAPbI_3$ network	650 nm	0.1	1.0×10^{12}	ref 66
$MAPbI_3$ nanonet	White light	0.6		ref 67
	700 nm	10.3		
$MAPbI_3$ nanoflake	265 nm	12.0	1.0×10^{11}	ref 68
$MAPbI_3$ porous photonic crystals	White light	12.7	3.2×10^{13}	ref 69

incident light. On the contrary, the electric field distribution on the flat substrate remains unchanged and is uniform (Figure 3j). Therefore, introducing a nanopillar array structure into the $MAPbI_3$ film can increase its light absorption and sensitivity, which is consistent with the experimental results.

3.4. Application of Image Sensors. Photodetectors are widely used in the field of image sensors. We have fabricated an image sensor composed of a 5 × 5 photodetector array. The size of each photodetector is 450 μm × 750 μm. As shown in Figure 4a, we used a hollowed out "T″-shaped metal mask (1.5 cm × 1.5 cm) and placed it on photodetectors to manufacture an image sensor. Figure 4b shows that the photoresponse of a single photodetector under white light at a bias voltage of 5.0 V is stable. When the light is turned off, the "T″ character cannot be recognized (Figure 4c) because all photodetectors display low dark current (<4.5×10^{-8} A). On the contrary, when the light is turned on, the photocurrent of all photodetectors below the character "T″ has significantly increased (>2.5×10^{-6} A), showing good resolution. Although due to incomplete shading, there is a small amount of light transmission, resulting in a slight increase (<3.5×10^{-7} A) in the current of the photodetector in the obstructed area; it is still much smaller than the photocurrent under direct illumination. Therefore, the character "T" can be recognized through mapping the photocurrent (Figure 4d).

4. CONCLUSIONS

In summary, we have prepared a large-area tunable SiO_2/Si nanopillar array via nanosphere lithography and dry etching and demonstrated its applications in improving the photosensitivity of perovskite materials. The SEM and XRD results indicate that the nanopillar array does not significantly decrease the crystallinity of $MAPbI_3$ thin films. Experimental results and COMSOL simulation results demonstrate that nanopillar arrays can improve light absorption and enhance the electric field within the nanopillar arrays covered by $MAPbI_3$ thin films, resulting in higher photosensitivity of $MAPbI_3$ thin films. The photodetector with nanopillar structures exhibited responsivity with 11.2 A/W and specific detectivity of 7.3×10^{10} Jones at 450 nm. In comparison to devices based on flat substrates, these photodetectors exhibit better light absorption ability in the visible light range, which is attributed to the light enhancement effect brought about by the nanopillar array structure. Additionally, an image sensor array was fabricated, and it demonstrated high-contrast image sensing. The nanopillar arrays are also suitable for other light-sensing materials such as InGaAs, GaN, CdS, and TiO_2.

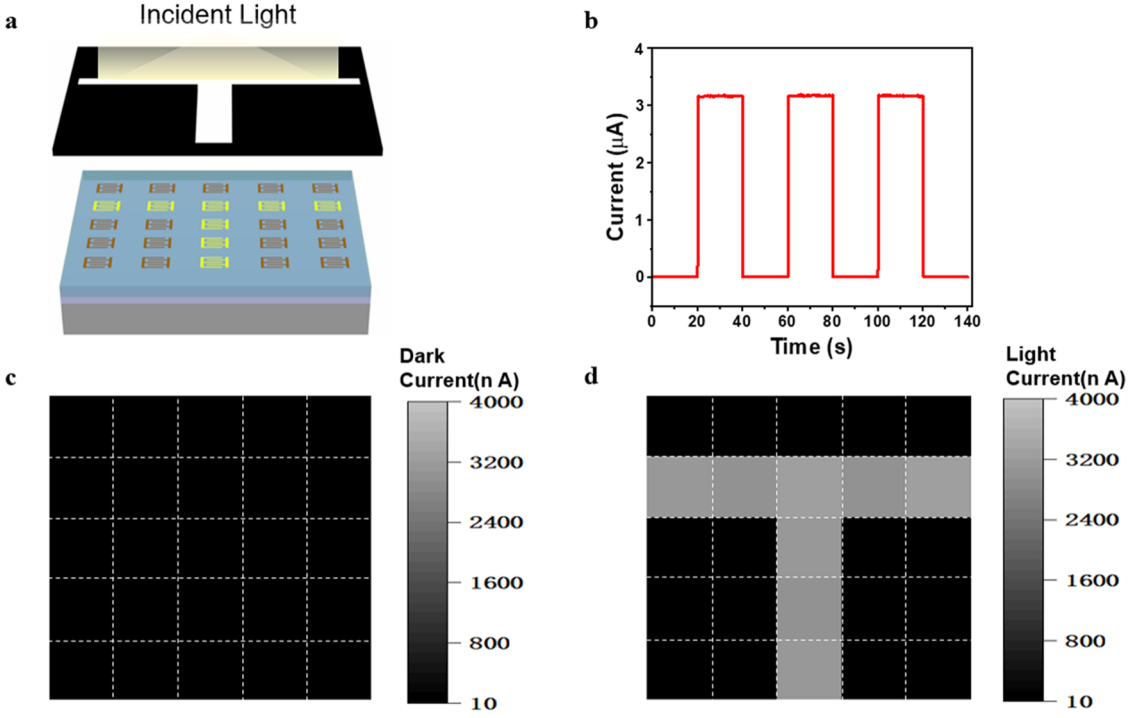

Figure 4. (a) Schematic illustration of a photodetector array with 5 × 5 pixels. (b) Time-resolved photoresponse of the photodetector based on a $MAPbI_3$ film on a SiO_2/Si nanopillar substrate (S-2 sample) under white light (1 mW/cm^2). (c, d) Output results of the photodetector array in darkness and under illumination, respectively.

https://doi.org/10.1021/acsomega.3c07390
ACS Omega 2024, 9, 2606−2614

■ ASSOCIATED CONTENT

Supporting Information

The Supporting Information is available free of charge at https://pubs.acs.org/doi/10.1021/acsomega.3c07390.

Materials and methods, Figures (S1−S12) include SEM images of periodic nanostructures (PS nanospheres, Si nanopillar arrays, SEM images of the $MAPbI_3$ film on flat and nanopillar substrates, single photodetector based on a $MAPbI_3$ film on a SiO_2/Si nanopillar substrate), images of $MAPbI_3$ thin-film spin-coated on a nanopillar array with different diameters, EDS of MAPbI3 film based on nanopillars substrate, dark/photocurrent of the photodetectors based on S-1 and S-3 samples, a histogram of the particle size distribution of $MAPbI_3$ film fabricated on the flat substrate and nanopillar substrate, photoluminescence spectra of the $MAPbI_3$ film in different substrates, and the $I-V$ test for S-2 after 72 h, with a light intensity of 1 mW/cm^2 under white light illumination (PDF)

■ AUTHOR INFORMATION

Corresponding Authors

Xiuzhen Xu − *Key Laboratory of Advanced Civil Engineering Materials of Ministry of Education, Key Laboratory of D&A for Metal-Functional Materials, School of Materials Science & Engineering, Tongji University, Shanghai 201804, China*; Email: xiuzhenxu@tongji.edu.cn

Jianhe Guo − *Guangdong Provincial Key Laboratory of Sensing Technology and Biomedical Instrument, School of Biomedical Engineering, Shenzhen Campus of Sun Yat-Sen University, Shenzhen 518107, China*; Email: guojianhe@mail.sysu.edu.cn

Wen Li − *Key Laboratory of Advanced Civil Engineering Materials of Ministry of Education, Key Laboratory of D&A for Metal-Functional Materials, School of Materials Science & Engineering, Tongji University, Shanghai 201804, China*; orcid.org/0000-0001-8912-3792; Email: liwen@tongji.edu.cn

Xiaobin Xu − *Key Laboratory of Advanced Civil Engineering Materials of Ministry of Education, Key Laboratory of D&A for Metal-Functional Materials, School of Materials Science & Engineering, Tongji University, Shanghai 201804, China*; orcid.org/0000-0002-3479-0130; Email: xiaobinxu@tongji.edu.cn

Authors

Zhengtong Yao − *Key Laboratory of Advanced Civil Engineering Materials of Ministry of Education, Key Laboratory of D&A for Metal-Functional Materials, School of Materials Science & Engineering, Tongji University, Shanghai 201804, China*

Yuting Xiong − *Key Laboratory of Advanced Civil Engineering Materials of Ministry of Education, Key Laboratory of D&A for Metal-Functional Materials, School of Materials Science & Engineering, Tongji University, Shanghai 201804, China*

Hanyue Kang − *Key Laboratory of Advanced Civil Engineering Materials of Ministry of Education, Key Laboratory of D&A for Metal-Functional Materials, School of Materials Science & Engineering, Tongji University, Shanghai 201804, China*

Complete contact information is available at: https://pubs.acs.org/10.1021/acsomega.3c07390

Author Contributions

Xiaobin Xu, W. L., Xiuzhen Xu, J. G., and Z.Y. conceived the idea. Xiaobin Xu, Dr. Xiuzhen Xu, and W.L. supervised the experiment. Z.Y. and H.K. performed the nanostructure fabrication and characterization. Y.X. and Xiuzhen Xu assisted in the photoelectric measurements. The data analyses were done through the contributions of all the authors. The manuscript was written through the contributions of all authors.

Notes

The authors declare no competing financial interest.

■ ACKNOWLEDGMENTS

The authors gratefully acknowledge the support from the National Natural Science Foundation of China (Grant No. 51901159) and the Fundamental Research Funds for the Central Universities.

■ REFERENCES

(1) Wang, F.; Zou, X. M.; Xu, M. J.; Wang, H.; Wang, H. L.; Guo, H. J.; Guo, J. X.; Wang, P.; Peng, M.; Wang, Z.; et al. Recent Progress on Electrical and Optical Manipulations of Perovskite Photodetectors. *Adv. Sci.* **2021**, *8*, No. 2100569.

(2) Yan, T. T.; Li, Z. Q.; Cao, F.; Chen, J. X.; Wu, L. M.; Fang, X. S. An All-Organic Self-Powered Photodetector with Ultraflexible Dual-Polarity Output for Biosignal Detection. *Adv. Mater.* **2022**, *34*, No. 2201303.

(3) Xu, Y. L.; Lin, Q. Q. Photodetectors based on solution-processable semiconductors: Recent advances and perspectives. *Appl. Phys. Rev.* **2020**, *7*, No. 011315.

(4) Cai, S.; Xu, X.; Yang, W.; Chen, J.; Fang, X. Materials and Designs for Wearable Photodetectors. *Adv. Mater.* **2019**, *31*, No. 1808138.

(5) Long, M.; Wang, P.; Fang, H.; Hu, W. Progress, Challenges, and Opportunities for 2D Material Based Photodetectors. *Adv. Funct. Mater.* **2019**, *29*, No. 1803807.

(6) Zhao, Z. J.; Xu, C. Y.; Ma, Y.; Yang, K. X.; Liu, M.; Zhu, X. X.; Zhou, Z. J.; Shen, L.; Yuan, G. C.; Zhang, F. J. Ultraviolet Narrowband Photomultiplication Type Organic Photodetectors with Fabry-Perot Resonator Architecture. *Adv. Funct. Mater.* **2022**, *32*, No. 2203606.

(7) Wang, Q. H.; Kalantar-Zadeh, K.; Kis, A.; Coleman, J. N.; Strano, M. S. Electronics and optoelectronics of two-dimensional transition metal dichalcogenides. *Nat. Nanotechnol.* **2012**, *7*, 699−712.

(8) Koppens, F. H. L.; Mueller, T.; Avouris, P.; Ferrari, A. C.; Vitiello, M. S.; Polini, M. Photodetectors based on graphene, other two-dimensional materials and hybrid systems. *Nat. Nanotechnol.* **2014**, *9*, 780−793.

(9) Lin, H.; Sturmberg, B. C. P.; Lin, K. T.; Yang, Y. Y.; Zheng, X. R.; Chong, T. K.; de Sterke, C. M.; Jia, B. H. A 90-nm-thick graphene metamaterial for strong and extremely broadband absorption of unpolarized light. *Nat. Photonics* **2019**, *13*, 270−276.

(10) Liu, M. X.; Yazdani, N.; Yarema, M.; Jansen, M.; Wood, V.; Sargent, E. H. Colloidal quantum dot electronics. *Nat. Electron.* **2021**, *4*, 548−558.

(11) Sulaman, M.; Yang, S. Y.; Bukhtiar, A.; Tang, P. Y.; Zhang, Z. H.; Song, Y.; Imran, A.; Jiang, Y. R.; Cui, Y. Y.; Tang, L. B.; Zou, B. Hybrid Bulk-Heterojunction of Colloidal Quantum Dots and Mixed-Halide Perovskite Nanocrystals for High-Performance Self-Powered Broadband Photodetectors. *Adv. Funct. Mater.* **2022**, *32*, No. 2201527.

(12) Lu, C. H.; Biesold, G. V.; Liu, Y. J.; Kang, Z. T.; Lin, Z. Q. Doping and ion substitution in colloidal metal halide perovskite nanocrystals. *Chem. Soc. Rev.* **2020**, *49*, 4953−5007.

(13) Li, Z. L.; Li, Z. Q.; Zuo, C. L.; Fang, X. S. Application of Nanostructured TiO_2 in UV Photodetectors: A Review. *Adv. Mater.* **2022**, *34*, No. 2109083.

(14) Ouyang, W. X.; Chen, J. X.; Shi, Z. F.; Fang, X. S. Self-powered UV photodetectors based on ZnO nanomaterials. *Appl. Phys. Rev.* **2021**, *8*, No. 031315.
(15) Zhao, B.; Wang, F.; Chen, H. Y.; Zheng, L. X.; Su, L. X.; Zhao, D. X.; Fang, X. S. An Ultrahigh Responsivity (9.7 mA W^{-1}) Self-Powered Solar-Blind Photodetector Based on Individual ZnO-Ga_2O_3 Heterostructures. *Adv. Funct. Mater.* **2017**, *27*, No. 1700264.
(16) Wang, H. P.; Li, S. Y.; Liu, X. Y.; Shi, Z. F.; Fang, X. S.; He, J. H. Low-Dimensional Metal Halide Perovskite Photodetectors. *Adv. Mater.* **2021**, *33*, No. 2003309.
(17) Chen, F. T.; Li, C. Q.; Shang, C. Y.; Wang, K. Y.; Huang, Q.; Zhao, Q. Q.; Zhu, H. L.; Ding, J. X. Ultrafast Response of Centimeter Scale Thin CsPbBr3 Single Crystal Film Photodetector for Optical Communication. *Small* **2022**, *18*, No. 2203565.
(18) Leng, K.; Abdelwahab, I.; Verzhbitskiy, I.; Telychko, M.; Chu, L. Q.; Fu, W.; Chi, X.; Guo, N.; Chen, Z. H.; Chen, Z. X.; et al. Molecularly thin two-dimensional hybrid perovskites with tunable optoelectronic properties due to reversible surface relaxation. *Nat. Mater.* **2018**, *17*, 908−914.
(19) Zhou, C. K.; Lin, H. R.; He, Q. Q.; Xu, L. J.; Worku, M.; Chaaban, M.; Lee, S.; Shi, X. Q.; Du, M. H.; Ma, B. W. Low dimensional metal halide perovskites and hybrids. *Mater. Sci. Eng., R* **2019**, *137*, 38−65.
(20) Zhao, Y. X.; Zhu, K. Organic-inorganic hybrid lead halide perovskites for optoelectronic and electronic applications. *Chem. Soc. Rev.* **2016**, *45*, 655−689.
(21) Zhang, F.; Lu, H. P.; Tong, J. H.; Berry, J. J.; Beard, M. C.; Zhu, K. Advances in two-dimensional organic-inorganic hybrid perovskites. *Energy Environ. Sci.* **2020**, *13*, 1154−1186.
(22) Zhu, F.; Lian, G.; Yu, B. C.; Zhang, T.; Zhang, L.; Yu, H. H.; Cui, D. L.; Wang, Q. L.; Zhang, H. J.; Meng, Q. B.; Wong, C. P. Pressure-Enhanced Vertical Orientation and Compositional Control of Ruddlesden-Popper Perovskites for Efficient and Stable Solar Cells and Self-Powered Photodetectors. *ACS Appl. Mater. Interfaces* **2022**, *14*, 1526−1536.
(23) Zhao, C. Z.; Xu, X. B.; Ferhan, A. R.; Chiang, N. H.; Jackman, J. A.; Yang, Q.; Liu, W. F.; Andrews, A. M.; Cho, N. J.; Weiss, P. S. Scalable Fabrication of Quasi-One-Dimensional Gold Nanoribbons for Plasmonic Sensing. *Nano Lett.* **2020**, *20*, 1747−1754.
(24) Zhang, Y. X.; Liu, Y. C.; Yang, Z.; Chen, M.; Liu, S. Z. Direct Growth of Pyramid-Textured Perovskite Single Crystals: A New Strategy for Enhanced Optoelectronic Performance. *Adv. Funct. Mater.* **2020**, *30*, No. 2002742.
(25) Fan, L. B.; Pei, Z. F.; Wang, P.; Zheng, Z. Research Progress on the Stability of Organic-Inorganic Halide Perovskite Photodetectors in a Humid Environment Through the Modification of Perovskite Layers. *J. Electron. Mater.* **2022**, *51*, 2801−2818.
(26) Zhu, P. C.; Gu, S.; Luo, X.; Gao, Y.; Li, S. L.; Zhu, J.; Tan, H. R. Simultaneous Contact and Grain-Boundary Passivation in Planar Perovskite Solar Cells Using SnO2-KCl Composite Electron Transport Layer. *Adv. Energy Mater.* **2020**, *10*, No. 1903083.
(27) Wang, H. R.; Zhang, X. Y.; Wu, Q. Q.; Cao, F.; Yang, D. W.; Shang, Y. Q.; Ning, Z. J.; Zhang, W.; Zheng, W. T.; Yan, Y. F.; et al. Trifluoroacetate induced small-grained CsPbBr3 perovskite films result in efficient and stable light-emitting devices. *Nat. Commun.* **2019**, *10*, No. 665.
(28) Mohd Yusoff, A. R. b.; Vasilopoulou, M.; Georgiadou, D. G.; Palilis, L. C.; Abate, A.; Nazeeruddin, M. K. Passivation and process engineering approaches of halide perovskite films for high efficiency and stability perovskite solar cells. *Energy Environ. Sci.* **2021**, *14*, 2906−2953.
(29) Liu, Y. C.; Zhang, Y. X.; Yang, Z.; Yang, D.; Ren, X. D.; Pang, L. Q.; Liu, S. Z. Thinness- and Shape-Controlled Growth for Ultrathin Single-Crystalline Perovskite Wafers for Mass Production of Superior Photoelectronic Devices. *Adv. Mater.* **2016**, *28*, 9204−9209.
(30) Jeong, J.; Kim, M.; Seo, J.; Lu, H. Z.; Ahlawat, P.; Mishra, A.; Yang, Y. G.; Hope, M. A.; Eickemeyer, F. T.; Kim, M. Pseudo-halide anion engineering for alpha-FAPbI(3) perovskite solar cells. *Nature* **2021**, *592*, 381−385.
(31) Wu, D. J.; Xu, Y. C.; Zhou, H.; Feng, X.; Zhang, J. Q.; Pan, X. Y.; Gao, Z.; Wang, R.; Ma, G. K.; Tao, L.; et al. Ultrasensitive, flexible perovskite nanowire photodetectors with long-term stability exceeding 5000 h. *InfoMat* **2022**, *4*, No. e12320.
(32) Bao, C. X.; Yang, J.; Bai, S.; Xu, W. D.; Yan, Z. B.; Xu, Q. Y.; Liu, J. M.; Zhang, W. J.; Gao, F. High Performance and Stable All-Inorganic Metal Halide Perovskite-Based Photodetectors for Optical Communication Applications. *Adv. Mater.* **2018**, *30*, No. 183422.
(33) Li, S. X.; Xia, H.; Wang, L.; Sun, X. C.; An, Y.; Zhu, H.; Bai, B. F.; Sun, H. B. Self-Powered and Flexible Photodetector with High Polarization Sensitivity Based on MAPbBr(3)-MAPbI(3) Microwire Lateral Heterojunction. *Adv. Funct. Mater.* **2022**, *32*, No. 2206999.
(34) Xu, X. Z.; Liu, W. F.; Ji, Z. K.; Hao, D. D.; Yan, W. Y.; Ye, Z. L.; Hu, Y.; Fang, M. H.; Wang, C. C.; Ma, L.; et al. Large-Area Periodic Organic-Inorganic Hybrid Perovskite Nanopyramid Arrays for High-Performance Photodetector and Image Sensor Applications. *ACS Mater. Lett.* **2021**, *3*, 1189−1196.
(35) Mao, J.; Sha, W. E. I.; Zhang, H.; Ren, X. G.; Zhuang, J. Q.; Roy, V. A. L.; Wong, K. S.; Choy, W. C. H. Novel Direct Nanopatterning Approach to Fabricate Periodically Nanostructured Perovskite for Optoelectronic Applications. *Adv. Funct. Mater.* **2017**, *27*, No. 1606525.
(36) Lin, C. H.; Cheng, B.; Li, T. Y.; Retamal, J. R. D.; Wei, T. C.; Fu, H. C.; Fang, X. S.; He, J. H. Orthogonal Lithography for Halide Perovskite Optoelectronic Nanodevices. *ACS Nano* **2018**, *13*, 1168−1176.
(37) Lyashenko, D.; Perez, A.; Zakhidov, A. High-resolution patterning of organohalide lead perovskite pixels for photodetectors using orthogonal photolithography. *Phys. Status Solidi A* **2017**, *214*, No. 1600302.
(38) Zha, J. J.; Luo, M. C.; Ye, M.; Ahmed, T.; Yu, X. C.; Lien, D. H.; He, Q. Y.; Lei, D. Y.; Ho, J. C.; Bullock, J.; et al. Infrared Photodetectors Based on 2D Materials and Nanophotonics. *Adv. Funct. Mater.* **2022**, *32*, No. 2111970.
(39) Song, C. K.; Ye, B. Y.; Xu, J. Y.; Chen, J. H.; Shi, W.; Yu, C. P.; An, C. W.; Zhu, J. W.; Zhang, W. C. Large-Area Nanosphere Self-Assembly Monolayers for Periodic Surface Nanostructures with Ultrasensitive and Spatially Uniform SERS Sensing. *Small* **2022**, *18*, No. 2104202.
(40) Luo, S. H.; Mancini, A.; Wang, F.; Liu, J. Y.; Maier, S. A.; de Mello, J. C. High-Throughput Fabrication of Triangular Nanogap Arrays for Surface-Enhanced Raman Spectroscopy. *ACS Nano* **2022**, *16*, 7438−7447.
(41) Zhao, C. Z.; Xu, X. B.; Bae, S. H.; Yang, Q.; Liu, W. F.; Belling, J. N.; Cheung, K. M.; Rim, Y. S.; Yang, Y.; Andrews, A. M.; Weiss, P. S. Large-Area, Ultrathin Metal-Oxide Semiconductor Nanoribbon Arrays Fabricated by Chemical Lift-Off Lithography. *Nano Lett.* **2018**, *18*, 5590−5595.
(42) Zhao, C. Z.; Xu, X. B.; Yang, Q.; Man, T. X.; Jonas, S. J.; Schwartz, J. J.; Andrews, A. M.; Weiss, P. S. Self-Collapse Lithography. *Nano Lett.* **2017**, *17*, 5035−5042.
(43) Mendoza-Carreño, J.; Molet, P.; Otero-Martinez, C.; Alonso, M. I.; Polavarapu, L.; Mihi, A. Nanoimprinted 2D-Chiral Perovskite Nanocrystal Metasurfaces for Circularly Polarized Photoluminescence. *Adv. Mater.* **2023**, *35*, 2210477 DOI: 10.1002/adma.202210477.
(44) Deng, K. M.; Liu, Z. Z.; Wang, M.; Li, L. Nanoimprinted Grating-Embedded Perovskite Solar Cells with Improved Light Management. *Adv. Funct. Mater.* **2019**, *29*, No. 1900830.
(45) Kang, S. M.; Jang, S.; Lee, J. K.; Yoon, J.; Yoo, D. E.; Lee, J. W.; Choi, M.; Park, N. G. Moth-Eye TiO2 Layer for Improving Light Harvesting Efficiency in Perovskite Solar Cells. *Small* **2016**, *12*, 2443−2449.
(46) Xiong, Y.; Xu, X.; Chen, B.; Xu, X. Highly Crystalized MAPbX3 Perovskite Triangular Nanowire Arrays for Optoelectronic Applications. *Adv. Mater.* **2023**, DOI: 10.1002/adma.202310427.
(47) Wang, W. T.; Lu, L. S.; Lu, X. Y.; Liang, Z. B.; Tang, B. A.; Xie, Y. X. Laser-induced jigsaw-like graphene structure inspired by Oxalis corniculata Linn. leaf. *Bio-Des. Manuf.* **2022**, *5*, 700−713.

https://doi.org/10.1021/acsomega.3c07390
ACS Omega 2024, 9, 2606−2614

(48) Xiong, Y. T.; Kang, H. Y.; Zhou, H. Z.; Ma, L.; Xu, X. B. Recent progress on microfluidic devices with incorporated 1D nanostructures for enhanced extracellular vesicle (EV) separation. *Bio-Des. Manuf.* **2022**, *5*, 607−616.
(49) Heng, W. Z.; Yang, G.; Kim, W. S.; Xu, K. C. Emerging wearable flexible sensors for sweat analysis. *Bio-Des. Manuf.* **2022**, *5*, 64−84.
(50) Wang, H. L.; Haroldson, R.; Balachandran, B.; Zakhidov, A.; Sohal, S.; Chan, J. Y.; Zakhidov, A.; Hu, W. Nanoimprinted Perovskite Nanograting Photodetector with Improved Efficiency. *ACS Nano* **2016**, *10*, 10921−10928.
(51) Zhan, Y.; Wang, Y.; Cheng, Q. F.; Li, C.; Li, K. X.; Li, H. Z.; Peng, J. S.; Lu, B.; Wang, Y.; Song, Y. L.; et al. A Butterfly-Inspired Hierarchical Light-Trapping Structure towards a High-Performance Polarization-Sensitive Perovskite Photodetector. *Angew. Chem., Int. Ed.* **2019**, *58*, 16456−16462.
(52) Bouich, A.; Mari-Guaita, J.; Soucase, B. M.; Palacios, P. Bright future by enhancing the stability of methylammonium lead triiodide perovskites thin films through Rb, Cs and Li as dopants. *Mater. Res. Bull.* **2023**, *163*, No. 112213.
(53) Li, Y.; Lohr, P. J.; Segapeli, A.; Baltram, J.; Werner, D.; Allred, A.; Muralidharan, K.; Printz, A. D. Influence of Halides on the Interactions of Ammonium Acids with Metal Halide Perovskites. *ACS Appl. Mater. Interfaces* **2023**, *15*, 24387.
(54) Emelianov, N. A.; Ozerova, V. V.; Zhidkov, I. S.; Korchagin, D. V.; Shilov, G. V.; Litvinov, A. L.; Kurmaev, E. Z.; Frolova, L. A.; Aldoshin, S. M.; Troshin, P. A. Nanoscale Visualization of Photodegradation Dynamics of MAPbI(3)Perovskite Films. *J. Phys. Chem. Lett.* **2022**, *13*, 2744−2749.
(55) Zhan, Y.; Cheng, Q. F.; Song, Y. L.; Li, M. Z. Micro-Nano Structure Functionalized Perovskite Optoelectronics: From Structure Functionalities to Device Applications. *Adv. Funct. Mater.* **2022**, *32*, No. 2200385.
(56) Zhang, Y. Q.; Ma, Y.; Wang, Y. X.; Zhang, X. D.; Zuo, C. T.; Shen, L.; Ding, L. M. Lead-Free Perovskite Photodetectors: Progress, Challenges, and Opportunities. *Adv. Mater.* **2021**, *33* (26), 2006691 DOI: 10.1002/adma.202006691.
(57) Liu, W. Advances in Hybrid Nanolithography: Wafer-Scale Fabrication of 1D to 3D Micro- and Nanostructures. Dissertation/Thesis. <Go to ISI>://PQDT:50716726, 2022.
(58) Sanches, A. W. P.; da Silva, M. A. T.; Cordeiro, N. J. A.; Urbano, A.; Lourenço, S. A. Effect of intermediate phases on the optical properties of PbI_2-rich $CH_3NH_3PbI_3$ organic-inorganic hybrid perovskite. *Phys. Chem. Chem. Phys.* **2019**, *21*, 5253−5261.
(59) Kim, E. B.; Akhtar, M. S.; Shin, H. S.; Ameen, S.; Nazeeruddin, M. K. A review on two-dimensional(2D) and 2D-3D multidimensional perovskite solar cells: Perovskites structures, stability, and photovoltaic performances. *J. Photochem. Photobiol., C* **2021**, *48*, No. 100405.
(60) Zhou, J. C.; Huang, J. Photodetectors Based on Organic-Inorganic Hybrid Lead Halide Perovskites. *Adv. Sci.* **2018**, *5*, No. 1700256.
(61) Jing, H.; Peng, R. W.; Ma, R. M.; He, J.; Zhou, Y.; Yang, Z. Q.; Li, C. Y.; Liu, Y.; Guo, X. J.; Zhu, Y. Y.; et al. Flexible Ultrathin Single-Crystalline Perovskite Photodetector. *Nano Lett.* **2020**, *20*, 7144−7151.
(62) Wang, H.; Kim, D. H. Perovskite-based photodetectors: materials and devices. *Chem. Soc. Rev.* **2017**, *46*, 5204−5236.
(63) Fang, Y.; Huang, J. Resolving Weak Light of Sub-picowatt per Square Centimeter by Hybrid Perovskite Photodetectors Enabled by Noise Reduction. *Adv. Mater.* **2015**, *27*, 2804−2810.
(64) Bao, C. X.; Zhu, W. D.; Yang, J.; Li, F. M.; Gu, S.; Wang, Y. R. Q.; Yu, T.; Zhu, J.; Zhou, Y.; Zou, Z. G. Highly Flexible Self-Powered Organolead Trihalide Perovskite Photodetectors with Gold Nanowire Networks as Transparent Electrodes. *Acs Appl. Mater. Interfaces* **2016**, *8*, 23868−23875.
(65) Hu, X.; Zhang, X. D.; Liang, L.; Bao, J.; Li, S.; Yang, W. L.; Xie, Y. High-Performance Flexible Broadband Photodetector Based on Organolead Halide Perovskite. *Adv. Funct. Mater.* **2014**, *24*, 7373−7380.
(66) Deng, H.; Yang, X. K.; Dong, D. D.; Li, B.; Yang, D.; Yuan, S. J.; Qiao, K. K.; Cheng, Y. B.; Tang, J.; Song, H. S. Flexible and Semitransparent Organolead Triiodide Perovskite Network Photodetector Arrays with High Stability. *Nano Lett.* **2015**, *15*, 7963−7969.
(67) Wang, W.; Ma, Y.; Qi, L. High-Performance Photodetectors Based on Organometal Halide Perovskite Nanonets. *Adv. Funct. Mater.* **2017**, *27*, No. 1603653.
(68) Zheng, W.; Lin, R. C.; Zhang, Z. J.; Liao, Q. X.; Liu, J. J.; Huang, F. An ultrafast-temporally-responsive flexible photodetector with high sensitivity based on high-crystallinity organic-inorganic perovskite nanoflake. *Nanoscale* **2017**, *9*, 12718−12726.
(69) Zhan, Y.; Wang, Y.; Cheng, Q.; Li, C.; Li, K.; Li, H.; Peng, J.; Lu, B.; Wang, Y.; Song, Y.; et al. A Butterfly-Inspired Hierarchical Light-Trapping Structure towards a High-Performance Polarization-Sensitive Perovskite Photodetector. *Angew. Chem., Int. Ed.* **2019**, *58*, 16456−16462.

https://doi.org/10.1021/acsomega.3c07390
ACS Omega 2024, 9, 2606−2614